Supporting Information

Fernandes et al. 10.1073/pnas.1108942108

SI Materials and Methods

Materials. For the ^{13}C NMR relaxation experiments a three-stage extraction process was used to isolate cellulose from microtome sections prepared from mature earlywood of Sitka spruce. Approximately 40 sections were placed in 8 mL H_2O and heated to 70 °C under gentle shaking. Delignification was started by adding 25 μL acetic acid and subsequently 75 mg sodium chlorite (i.e., 93.7 mg 80% $NaClO_2$). After 1 h, 2 h, and 4 h the same amount of delignifying agents were added. Hemicelluloses (predominately xylans) and residual lignin were removed from the sections by a mild alkali extraction in 6.5% KOH at 20 °C under N_2 atmosphere and gentle shaking (1). After 4 h the sections were placed in cold water overnight. The remaining hemicelluloses (mainly glucomannan) were removed by hydrolysis in 2.5 M HCl at 100 °C under gentle shaking in closed vials (2). Monosaccharide composition after total acid hydrolysis was determined by HPLC (3) and led to estimates of 53% cellulose, 11% glucomannan, and 7% xylan in the wood.

Small-Angle Neutron Scattering (SANS). The contrast-matching solvent composition was derived as follows. Scattering length densities of H_2O and D_2O are widely reported (-0.56×10^{10} cm^{-2} and 6.35×10^{10} cm^{-2} respectively). For cellulose, the scattering length density has been reported as 1.86×10^{10} cm^{-2} (4), and 1.74×10^{10} cm^{-2} (5), which are similar. Using the value from (4) the scattering length density of cellulose can be matched using a solution comprising a 35:65 D_2O:H_2O ratio.

Wide-Angle X-Ray Scattering (WAXS). Background correction was carried out in three stages: (*i*) For encapsulated, hydrated samples the scattering pattern from the encapsulation film was subtracted, then for samples containing more than the saturation content of water an isotropic diffraction pattern measured for bulk water was scaled to fit and subtracted; (*ii*) A radial plot of azimuthal minima was constructed; and (*iii*) a dual-exponential function was fitted to these minima, assumed to be isotropic and subtracted.

The radial profiles of the 1–10, 110, 200, and 400 reflections were each fitted with an asymmetric function of the form:

$$I = 0.399 I_o(1 + f(q)) \exp(-0.5((q\text{-}q_o)/\sigma)^2/\sigma,$$

where I_o is the maximum intensity located at $q = q_o$ and $f(q) = a(q\text{-}q_o)^2$ when $q < q_o$ but zero when $q > q_o$. This function is based on a Gaussian profile with asymmetry introduced by the term $f(q)$ and controlled in magnitude by the fitted constant a. There has been extensive discussion of the most appropriate function to describe broadening in diffraction experiments of this type, where the contributions from disorder and limited lattice dimensions are theoretically assigned Gaussian and Cauchy profiles (6, 7). The difference between these symmetric models was relatively small. However the introduction of asymmetry into the modeled profile allowed much closer fits to the data than any symmetric function. The asymmetry term $f(q)$ expresses a specific form of disorder in which a distribution of d-spacings wider than the predominant ones are present.

Instrumental broadening was measured experimentally using powdered (<10 μm) lanthanum hexaboride. For each reflection the observed σ value was corrected for instrumental broadening by ${\sigma_{obs}}^2 = ({\sigma_{corr}}^2 + {\sigma_{instr}}^2)^{0.5}$ and was used to calculate the full width at half maximum $F = 2.355\ \sigma_{corr}$., from which the Scherrer dimensions and disorder factors were determined.

Deuteration-FTIR Microscopy. Longitudinal-tangential 20 μm sections were used for transmission FTIR in a Thermo Nicolet Nexus Spectrometer equipped with a Nicolet Continuum microscope attachment, with a liquid-nitrogen-cooled MCT detector. The scanning parameters used were: resolution, 4 cm^{-1}; number of scans, 128. Aperture sizes varied according to the dimensions of the section but were always at least 25 μm in each dimension to minimize distortion of the spectra by scattering effects. For vapor-phase deuteration experiments the sample was enclosed in a through-flow cell with upper and lower windows of BaF_2. The sample had to be retained free from back-exchange with traces of H_2O while the deuterated spectrum was measured. Preventing back-exchange is technically difficult with samples thin enough for transmission FTIR (8, 9). A stream of nitrogen or air, predried over molecular sieve, was passed through either a drying tube filled with phosphorus pentoxide (Sicapent, Aldrich) or a bubbling tube filled with D_2O. The nitrogen line was arranged to allow switching between the drying and deuteration modes without exposure to the atmosphere.

Single-Pulse-Excitation (SP-MAS) ^{13}C NMR. The MOST (Measurement of Short T_1s) experiment was carried out with a ^{13}C pulse duration of 4 μs and short recycle times of 0.1–12.8 s to edit out rigid components with ^{13}C spin-lattice relaxation time T_1 substantially longer than these. The SP-MAS spectrum was deconvoluted into Gaussian components corresponding to each signal including those at 66, 62, and 61 pm assigned to the *tg*, *gt*, and *gg* C-6 orientations. The evolution of signal intensity with recycle time was modeled by least-squares fitting to dual-exponential functions with the relative total signal intensities derived from the cross polarization, magic-angle spinning (CP-MAS) spectrum. A background signal at 111 ppm was derived from the Teflon rotor caps.

Proton Spin-Diffusion NMR: 2D Representation of the Goldman-Shen Experiment. The pulse sequence for the ^1H T_2-based form of the experiment was as described previously (3). Using $H_i =$ the amplitude $(h\text{-}h')/h_0$ in the notation of (10), the 2D spectrum $H(i,j) = abs(\Sigma(\tau = 0 \rightarrow 5.2\ \text{ms})\ (H_i\text{-}H_j)$ where τ is the time allowed for spin diffusion. This function corresponds to the area enclosed between the spin equilibration curves for signals i and j up to an equilibration time of 5.2 ms, indicating spatial separation if i and j were initially magnetically distinct. Alternatively, the reciprocal of the area enclosed between pairs of equilibration curves could have been used to give cross peaks indicating spatial proximity, but this representation would be potentially misleading because it could also indicate coincidental equality in initial magnetization, as might result from similar mobilities in two domains distant from one another.

1. Salmen L, Olsson AM (1998) Interaction between hemicelluloses, lignin and cellulose: Structure-property relationships. *Journal of Pulp and Paper Science* 24:99–103.
2. Liitia T, Maunu SL, Hortling B, Tamminen T, Pekkala O, et al. (2003) Cellulose crystallinity and ordering of hemicelluloses in pine and birch pulps as revealed by solid-state NMR spectroscopic methods. *Cellulose* 10:307–316.
3. Altaner C, Apperley DC, Jarvis MC (2006) Spatial relationships between polymers in Sitka spruce: proton spin-diffusion studies. *Holzforschung* 60:665–673.
4. Crawshaw J, Vickers ME, Briggs NP, Heenan RK, Cameron RE (2000) The hydration of TENCEL® cellulose fibres studied using contrast variation in small-angle neutron scattering. *Polymer* 41:1873–1881.

5. Evmenenko G, Alexeev V, Reynaers H (2000) Structural study of polysaccharide films by small-angle neutron scattering. *Polymer* 41:1947–1951.
6. Samir OM, Somashekar R (2007) Intrinsic strain effect on crystal and molecular structure of (dch32) cotton fiber. *Powder Diffraction* 22:20–26.
7. Thygesen A, Oddershede J, Lilholt H, Thomsen AB, Stahl K (2005) On the determination of crystallinity and cellulose content in plant fibres. *Cellulose* 12:563–576.
8. Marechal Y, Chanzy H (2000) The hydrogen bond network in I-beta cellulose as observed by infrared spectrometry. *Journal of Molecular Structure* 523:183–196.
9. Sturcova A, His I, Apperley DC, Sugiyama J, Jarvis MC (2004) Structural details of crystalline cellulose from higher plants. *Biomacromolecules* 5:1333–1339.
10. Newman RH (1992) Nuclear magnetic resonance study of spatial relationships between chemical components in wood cell walls. *Holzforschung* 46:205–210.

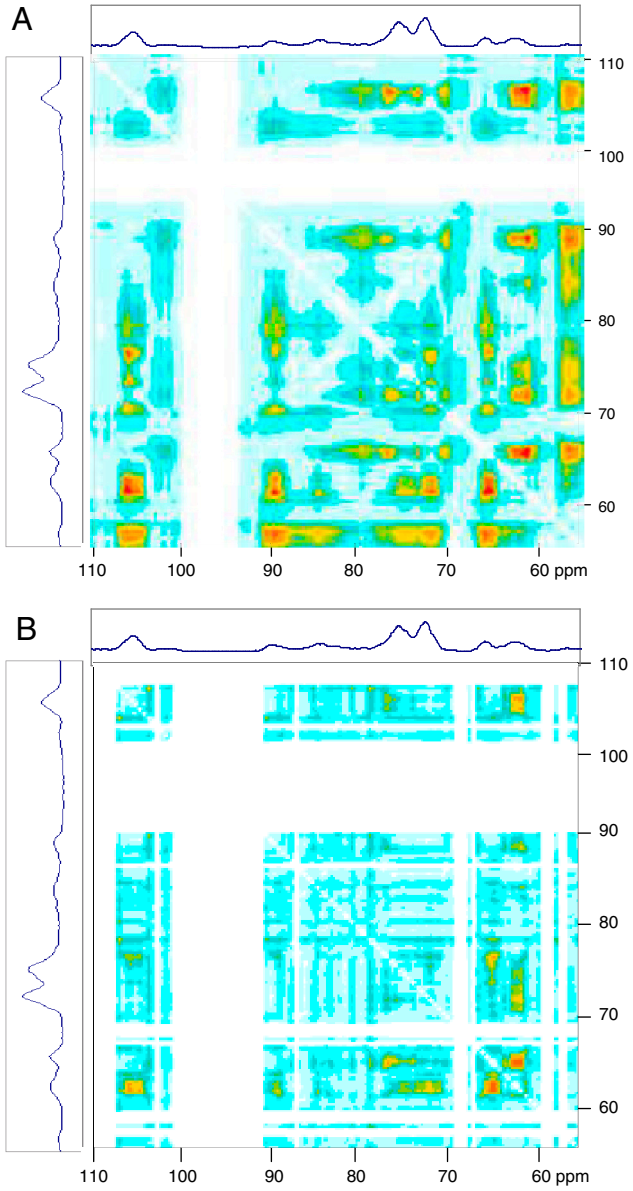

Fig. S1. 2D proton spin-diffusion spectra. (*A*). Spectrum from Sitka spruce latewood, with the initial spin disequilibrium established using differences in ^{1}H spin-spin relaxation as described for earlywood in the *Materials and Methods* section in the main text. (*B*). Spectrum from Sitka spruce latewood, with the initial spin disequilibrium established by a ^{1}H spin-locked delay of 100 μs to exploit differences in ^{1}H rotating-frame spin-lattice relaxation. The signal-noise ratio in (*B*) was inferior due to dissipation of spin disequilibrium during the delay period.

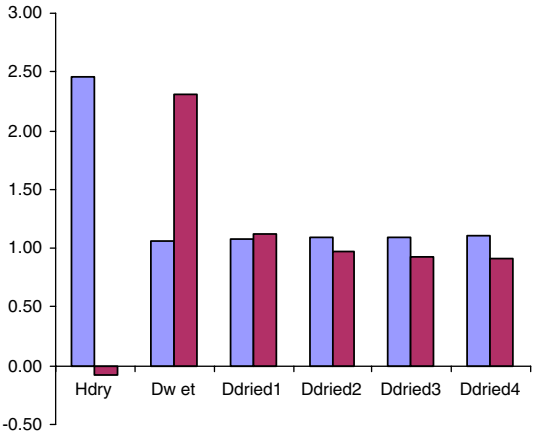

Fig. S2. Deuteration and drying of Sitka spruce earlywood, showing that stable deuteration was maintained during exhaustive drying. Intensity of the O-H stretching region (blue) integrated between 3,020 and 3,710 cm^{-1} in the transmission FTIR spectra, and of the O-D stretching region (red) integrated between 2,300 and 2,760 cm^{-1}. Intensities were normalized relative to the integrated intensity of the C-H stretching bands, which are not affected by deuterium exchange. The initial data point (Hdry) is after drying the section prior to deuteration. Spectra could not be recorded while the sample was being presoaked in liquid D_2O, due to the excessive D_2O absorbance. The sample was dried in flowing ultradry air and spectra (Ddried1-4) were recorded at 10 min intervals after the first point (Dwet) where enough D_2O had been removed for adequate transmission.

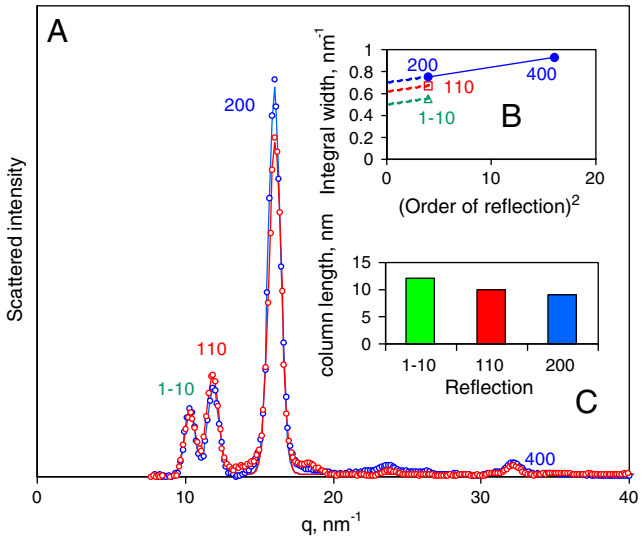

Fig. S3. Wide-angle X-ray scattering from *Valonia* cellulose. (*A*). Equatorial scattering profile collected under similar conditions to the data from Spruce cellulose; (*B*). Plot of the radial width of each reflection against $(\text{reflection order})^2$. The slope of the plot (assumed linear) gives the disorder parameter $g = 0.02$ in the (200) direction and the weighted-mean column length is calculated from the intercept by the Scherrer equation. Column lengths for the three main equatorial reflections, assuming that g is constant, are shown in (*C*) and were greater in the directions normal to the (1–10) and (110) lattice planes than normal to the (200) lattice plane. This relationship is as predicted for the well established diamond shape of *Valonia* cellulose microfibrils, which have the (1–10) and (110) lattice planes exposed at the surface, and was the reverse of what was observed for spruce cellulose. The oriented *Valonia* cellulose sample was a kind gift from Prof. J. Sugiyama.